

The influence of nitrogen content on the properties of TiN_x thin films

D. MUNTEANU*, F. VAZ^a

Dept. of Technological Equipment and Materials Science, Transilvania University, 29 Eroilor Blvd., 500036 Brasov, Romania

^a*Dept. of Physics, Minho University, 4800 – 058 Guimarães, Portugal*

Within the frame of this work, the TiN_x samples were deposited by reactive dc magnetron sputtering, from a high purity Ti target onto polished high-speed steel (AISI M2). The nitrogen content varies between 0 and 55 at.%. X-ray diffraction showed the development of the hexagonal α -Ti phase, with strong [002] orientation, for low nitrogen contents. For nitrogen contents of 20 and 30 at.%, the ϵ - Ti_2N phase appears with [200] orientation. With further increasing the nitrogen content, the δ -TiN phase becomes dominant. With increasing nitrogen content the films become harder, varying from about 8 GPa for pure titanium up to 27 GPa for a nitrogen content of 30 at.%. The hardness remains constant with a value of about 20 GPa within the range of 45 and 55 at.% N. A similar increase of residual stresses with nitrogen incorporation is observed.

(Received January 18, 2006; accepted March 23, 2006)

Keywords: Titanium nitride, Nitrides, Structural properties, Sputtering

1. Introduction

The continuous progress in surface and thin film technology is largely connected to the adjustment of structural and chemical film properties to actual applications. The resulting demands for increased sophistication of thin film structures can, in general, only be achieved by an appropriate choice and precise control over the parameters governing the deposition process. Besides the deposition parameters related with the film forming particle flux, stoichiometry of the deposited films has to be considered as one of the most essential parameter for determining the microstructural properties and chemical binding conditions of the growing film. In this respect, thin films elaborated through physical vapor deposition (PVD) processes are well known to exhibit a microstructure that is strongly dependent on these stoichiometric features [1-2].

In recent years there has been an increasing interest in elucidating the mechanisms, which lead to thin-film property modification caused by the so-called substoichiometric condition [3-8]. Much of our understanding of these structures and its relationships to their formation mechanism has come from the study of simple models by means of both computer simulation and theoretical methods [3-11]. This study is of major importance since a detailed understanding of the process reveals to be fundamental for the preparation of new materials and novel devices that exhibit improved physical properties [12-14].

Stoichiometric titanium nitride (TiN) is actually one of the most important technological coating material, not only because of its excellent tribological properties but also due to a good chemical stability. It is certainly, in

tribological terms, the most explored hard thin film material and most extensively used in industry. It is used in a wide range of applications, which range from protective material for machine parts and cutting tools [15] to diffusion barriers in semiconductor technology [16]. In the past, properties of substoichiometric titanium nitride (TiN_x) have been studied by comparably few researchers considering only basic properties such as hardness, phase composition or lattice distortion [17-23]. All these investigations focused mainly on the δ -TiN-phase, whereas little attention was paid to the properties of the nitrogen containing α -Ti phase. In this paper, we investigate the structural, physical and mechanical properties of substoichiometric TiN_x coatings aiming an accurate understanding of its evolution as a function of the increasing nitrogen content.

2. Experimental details

The TiN_x samples were deposited by reactive dc magnetron sputtering, from a high purity Ti target onto polished high-speed steel (AISI M2) and silicon substrates. The depositions were carried out in a "home-made" apparatus under Ar/ N_2 atmosphere [24]. The system consists of two vertically opposed rectangular magnetrons in a closed field configuration. The magnetron sources are unbalanced of type 2 [25]. Prior to depositions, the substrates were *ex situ* ultrasonically cleaned and *in situ* sputter etched for 15 min. in a pure Ar atmosphere, using a pulsed power supply: $I \approx 0.35$ A; $V \approx 300$ V; $f = 200$ kHz. A pure titanium adhesion layer (dc power source: $I = 1$ A, $V \approx 360$ V; $V_{\text{bias}} = -70$ V; $T_s \approx 250$ °C) with a thickness of ~ 0.40 μm was deposited on the substrate prior coating

deposition. The target to substrate distance was kept at 70 mm in all runs and the substrate holder was rotating over the targets at a constant frequency of 7 rpm. The base pressure in the deposition chamber was typically in the order of 10^{-4} Pa and rose to values around 4×10^{-1} Pa during depositions. Substrates were dc biased with a potential of -70 V and the temperature reached the value of about 250 °C during depositions. The experiments were carried out with the titanium target coupled to a dc power supply: $I = 1 \times 10^{-2}$ A/cm²; $V \approx 400$ V. The nitrogen partial pressure varied from 0 to 3×10^{-2} Pa corresponding to a flow rate variation from 0 (pure Ti coating) up to 8 sccm. An average number of 5 “ball cratering” (BC) experiments were carried out in each sample to determine its thickness.

X-ray diffraction (XRD) diffractograms have been recorded using a conventional SIEMENS D5000 diffractometer, working with a copper X-ray tube, a punctual detector and a forward graphite monochromator which avoids parasitic intensities (fluorescence) of Fe and Cr atoms from steel substrates.

Residual stresses, σ_r , were calculated from Stoney equation [26], using substrate curvature radii measured before and after coating deposition by scanning the sample surface with a laser beam and measuring the reflected light intensity (laser triangulation). The deflections of the surface used for the determination of the radius of curvature were measured with accuracy better than $1 \mu\text{m}$. The parabolic deflections correspond to orthogonal directions in the film surface plane [27].

Coating hardness was determined from the loading and unloading curves, carried out with an ultra low load depth sensing nanoindenter - Nano Instruments Nanoindenter II [28], equipped with a Berkovich diamond indenter and operating at a constant displacement rate of 5 nm/s until an indentation depth of 100 nm was reached. This indentation depth was kept within the recommended value of roughly 10 - 20 % of the film thickness to avoid substrate effect [29]. The unload segment is load controlled with an unloading rate equal to 50 % of the loading rate, at the end of the previous load segment. The unloading continues until 90 % of the previous load has been removed from the indenter. The experiment ends with a hold segment and a final unload segment in which 100 % of the load is removed. The elastic modulus of the films was estimated by the slope of the initial portion of the unloading curve, adopting Sneddon's flat-ended cylinder punch model [30]. Hardness values were obtained from the average of 20 measurements at different positions. Ten more measurements were performed for samples with greater dispersion in the results.

3. Results

A large number of samples were prepared in a wide range of N contents in order to perform an analysis as accurate as possible of the structural features that occurred with the deposition parameters variation (namely the nitrogen flow and thus as a function of the increasing content of this element). The dependence of coating

composition on nitrogen flow during the process was measured by RBS. Table 1 presents a summary of the analyzed coatings.

Table 1. Composition and thickness of the studied samples prepared with variation in the power applied to the Ti target.

Sample	Ti (at. %)	N (at. %)	Thickness (μm)
TiN 1	100	0	3.8 ± 0.4
TiN 2	98	2	3.9 ± 0.4
TiN 3	96	4	4.2 ± 0.4
TiN 4	92	8	3.0 ± 0.3
TiN 5	80	20	4.0 ± 0.4
TiN 6	70	30	2.9 ± 0.3
TiN 7	55	45	2.9 ± 0.3
TiN 8	50	50	1.9 ± 0.2
TiN 9	48	52	1.8 ± 0.2
TiN 10	45	55	1.7 ± 0.2

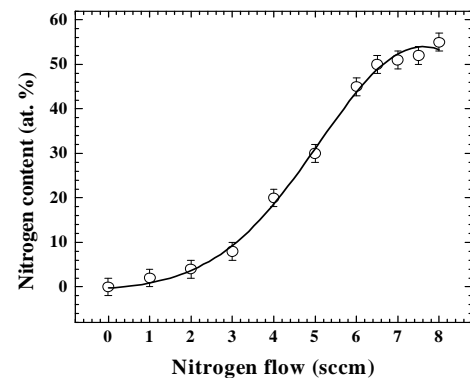


Fig. 1. The dependence of coating composition on nitrogen flow during the process (measured by RBS).

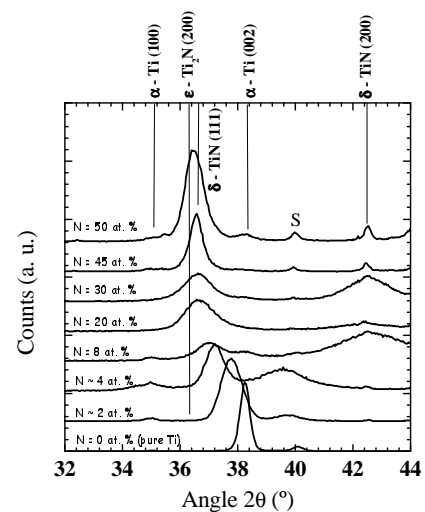


Fig. 2. The formation of the ϵ -Ti₂N phase as revealed by the XRD patterns.

The rapid increase in the N content that is observed here for nitrogen contents higher than 8 at. %, was also evidenced by other authors [21], and can be related to the formation of the ϵ -Ti₂N phase as revealed by the XRD patterns (Fig. 2) [31,32].

No oxygen and argon were detected in the as-deposited samples, which mean that their content is less than ~2 at. %. The dependence of coating composition on nitrogen flow during the process was measured by RBS and is illustrated in Fig. 1.

As the stoichiometric condition becomes closer and thus approaching the equilibrium condition, the deposition rates decrease as illustrated in Fig. 3. A certain nitrogen concentration leads to precipitation of an energetically more favorable lattice configuration, which in this case is the ϵ -Ti₂N phase or, by further increasing the nitrogen content, the δ -TiN phase, and thus there is a tendency for the decrease in the deposition rates.

The investigation of the coating morphology by SEM shows a columnar-type structure for all films (Fig. 4), lying in the transition zone between T and I zones of Thornton Model [35].

The initial hardening for the lowest N contents is a consequence of the distortion in the α -Ti lattice, due to N incorporation [32]. In fact, this lattice distortion, and the consequent increase in residual stresses can be observed in Fig. 6, which shows the evolution of the residual stresses with the N content. From this graph it is clear that all

coatings are in a high compressive stress state ranging from -3.2 down to -8 GPa.

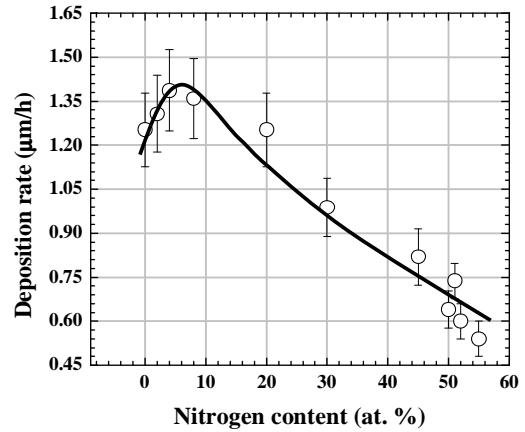


Fig. 3. An increase in deposition rate is observed for the films with the lowest N concentration (<10 at.%).

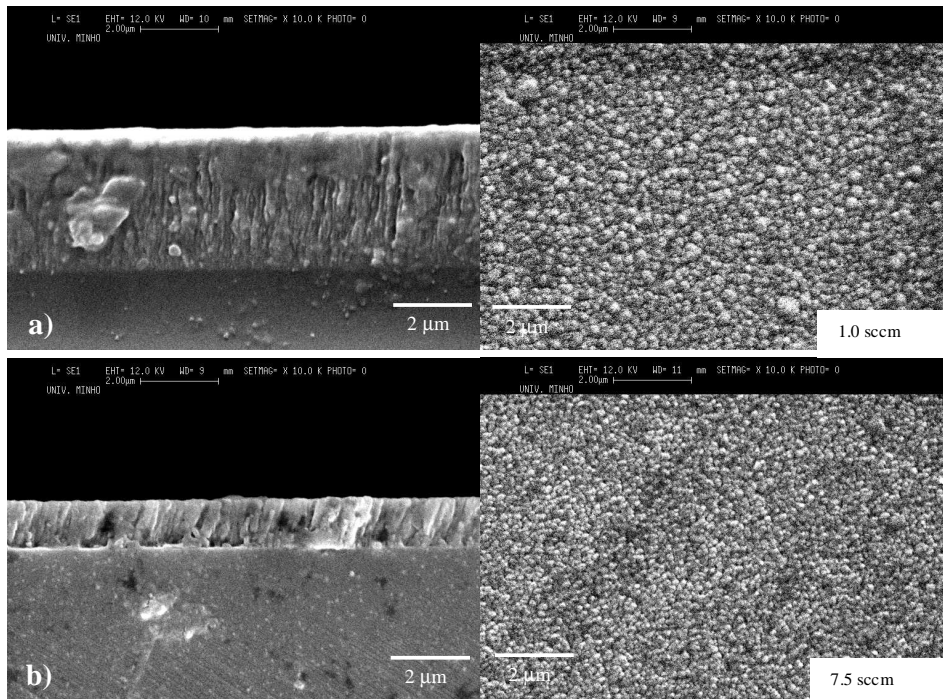


Fig. 4. The investigation of the coating morphology by SEM.

With increasing nitrogen content the films become harder, where the hardness value varies from about 8 GPa for pure titanium, up to 27 GPa for an optimal nitrogen content of 30 at.% (Fig. 5). It is worth noticing that films exhibit almost a constant hardness value of about 20 GPa within the range of 45 and 55 at.% N including stoichiometric TiN composition.

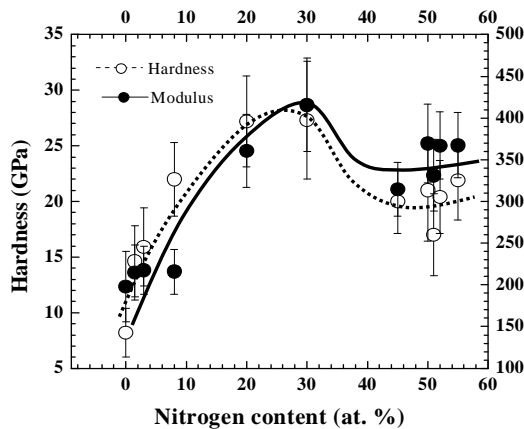


Fig. 5. The dependence of film hardness on nitrogen content.

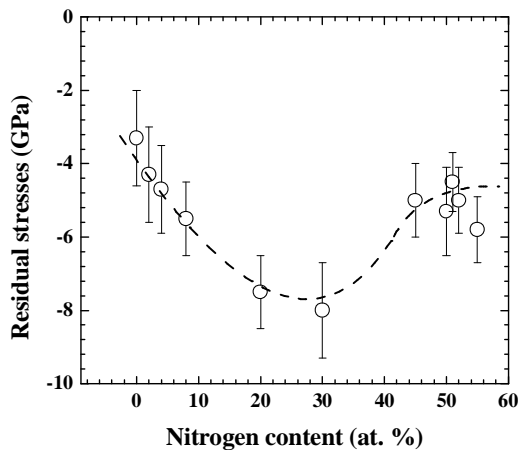


Fig. 6. The evolution of the residual stresses as function of nitrogen content.

4. Discussion

The nitrogen content first rises slowly from 0 to 8 at.%. Further increase of the nitrogen flow ratio leads to a steeper increase of the nitrogen content in the film up to 50 at.%, which corresponds to the stoichiometric situation, TiN. For higher flows, the nitrogen content rises only slightly. The investigation of substoichiometric titanium nitride films deposited by different PVD techniques shows

that increasing nitrogen flows and then the gas pressure during the deposition process leads to gradually higher nitrogen contents in the films [18,21].

Although the appearance of ϵ -Ti₂N phase is not clearly visible due to the influence of the diffraction peak corresponding to the {111} planes of δ -TiN phase, it seems nevertheless to be particularly evident for samples with 20 and 30 at.% N (as expected from the Ti-N phase diagram [31]). A closer look to the XRD diffraction patterns reveals the development of the hexagonal α -Ti phase with strong [002] orientation for low nitrogen contents (Fig. 2).

The diffraction peaks are progressively shifted towards lower diffraction angles as the N content increases. For nitrogen contents of 20 and 30 at.%, the ϵ -Ti₂N phase appears with a [200] orientation. Furthermore, and although it does not seem clearly visible, the δ -TiN phase might be already developing. The broad diffraction lines do not allow concluding unambiguously concerning the exact nature of the crystalline compounds present whereas the phase diagram predicts only the ϵ -Ti₂N phase as well as the α -Ti, but with diffraction peaks shifted to lower diffraction angles due to nitrogen insertion.

The titanium – nitrogen phase diagram is complex, but basically Ti crystal is said to be an "interstitial" crystal where N atoms fit into the gaps in the Ti structure. This structure evolves from hexagonal α -Ti (space group P6₃/mmc), to face-centered-cubic δ -TiN (space group P6₃/mmc), as the amount of nitrogen is increased. The α -Ti lattice is able to accept small amounts of nitrogen at octahedral sites [33], but since PVD is a thermodynamically non-equilibrium process, the α -Ti lattice may be forced to accept more nitrogen atoms due to hindered mobility of the deposited particles [19]. Therefore an oversaturated metastable solution of nitrogen in titanium is formed for the lower N contents.

The shift in the diffraction lines revealed by Fig. 2 is thus a consequence of this progressive increase of N interstitials in octahedral sites of α -Ti, which causes lattice distortion and thus diffraction peak broadening. At intermediate concentrations of N between 20 and 30 at.%, the diffraction peaks become quite broad indicating that grains of very small sizes and large micro strains are developed.

This tendency towards smaller grain sizes is typical of highly saturated metal-metalloid alloys and can be described by the Gibbs-Thomson equation [34]. Oversaturating under non-equilibrium conditions often leads to vanishing lattice order [17], inducing an increase in the deposition rates. This is the case here, as shown in Fig. 3, where an increase of deposition rate is observed for the films with the lowest N concentration (< 10 at. %).

A closer look at the different cross-section images reveals a clear tendency for the thickening of the columns (in the columnar structure zone) as the N content increases. Plan view observation also reveals some changes, namely in what concerns the surfaces roughness, which seems to decrease with the increase in the N content. The decrease in grain size explains the observed

densification of the initially columnar coating structure as well as the smoothening of the surface.

The overall observed behavior for the hardness is the result of two major contributions, corresponding to an initial increase till a maximum value in the region of 20 – 30 at.% N, and a slight decrease in the range of 30-45 at.% N contents. Two main factors may contribute for this increasing hardness of the TiN_x films: i) structure/composition (affected by the processing conditions) and ii) the lattice distortion [19,36,32].

In terms of the structural features, it is worth notice that the two harder samples are exactly those with the clear presence of the $\epsilon-Ti_2N$ phase, corresponding to 20 and 30 at.% N (see Fig. 3). The existence of this phase may act as a hardening factor [37-40]. This effect is presumed to be in the form of either: i) a precipitation nuclei, which rarely exhibit their own diffraction pattern and in such a case precipitation hardening effect is considered or, ii) very fine grains, which is probably the case here, taking in consideration the large broadening of the diffraction peaks of samples with 20 and 30 at.% N.

The formation of the $\delta - TiN$ phase, Fig. 3, and consequently a more stable and energetically favorable structure is expected to be followed by stress relieves, as it is the case illustrated in Fig. 7, for the samples with the highest N contents. Furthermore, plots of hardness variation with the compressive stress fields on Fig. 8, shows the existence of a relation ship between compressive stresses and hardness. The hardness increases almost linearly with increasing stresses, revealing that not only phase formation and composition play an important role, but also the lattice distortions related to structural defects and correspondent increases in intrinsic stresses are determinant for the hardening of the coatings.

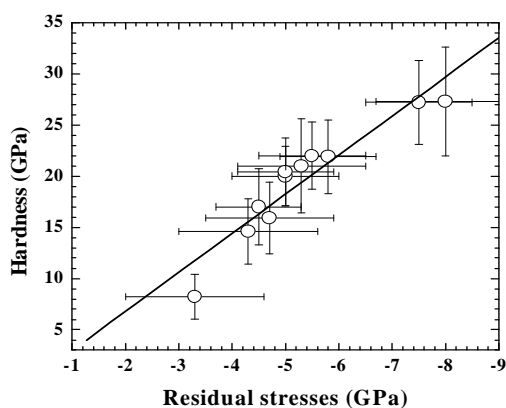


Fig. 7. The evolution of the residual stresses with the N at. %

5. Conclusions

Within the frame of this work, TiN films with a wide range of N contents were prepared in order to analyze the

structural and mechanical features that occurred with the variation of the nitrogen content. With the increase in the flow rate of the gas, the nitrogen content first rises slowly from 0 to 8 at.%. Further increasing the nitrogen flow ratio leads to a steeper increase of the coating nitrogen content up to 50 at.%, which corresponds to the stoichiometric compound, TiN. For higher flows, the nitrogen content rises only slightly.

XRD diffraction patterns reveal the development of the hexagonal $\alpha-Ti$ phase with strong [002] orientation for low nitrogen contents; the N atoms are distributed into octahedral sites. For nitrogen contents between 20 and 30 at.% the $\epsilon-Ti_2N$ phase appears with [200] orientation. Further increasing the nitrogen content, the $\delta-TiN$ phase appears. SEM micrographs show a columnar-type structure lying in the transition zone between T and I zones of Thornton Model for all films, with a clear tendency for the thickening of the columns as the N content increases.

With increasing nitrogen content the films become harder, varying from about 8 GPa for pure titanium up to 27 GPa for a nitrogen content of 30 at.%. The hardness remains constant with a value of about 20 GPa within the range of 45 and 55 at.% N. This behavior is mainly influenced by the two following contributions: i) structure/composition (affected by the processing conditions) and; ii) the lattice distortion and the correspondent increase in stresses. The two harder samples are those with the clear presence of the $\epsilon-Ti_2N$ phase, revealing a strong influence of crystalline structure in hardness behavior. Hardness also increases almost linearly with increasing stresses, revealing that the lattice distortions and the correspondent increases in intrinsic stresses are determinant for the hardening of the coatings.

References

- [1] J. A. Thornton, *J. Vac. Sci. Technol.* **11**, 666 (1974).
- [2] H. Oechsner, *J. Vac. Sci. Technol. A* **16**(3), 1956 (1998).
- [3] T. Takagi, *Thin Solid Films* **92**, 1 (1982).
- [4] P. J. Martin, *J. Mater. Sci.* **21**, 1 (1986).
- [5] D. N. Lee, *Journal of Materials Science* **24**, 4375 (1989).
- [6] K. H. Müller, *Physical review B*, **35**, **15**, 7906 (1987).
- [7] M. J. Brett, *J. Vac. Sci. Technol.* **A6** (3), 1749 (1988).
- [8] P. Meakin, P. Ramandal, L. M. Sander, R. C. Ball, *Physical Review A* **34** (6), 5091 (1986).
- [9] S. Hong, E. Kim, B. Bae, K. No, S. Lim, S. Woo, Y. Koh, *J. Vac. Sci. Technol. A* **14** (5), 2721 (1996).
- [10] A. Hamerich, R. Wunderlich, J. Muller, *J. Vac. Sci. Technol. A* **12** (5), 2873 (1994).
- [11] A. Kinbara, E. Kusano, S. baba, *J. Vac. Sci. Technol. A* **10** (4), 1483 (1992).
- [12] F. Vaz, L. Rebouta, S. Ramos, M. F. da Silva, J. C. Soares, *Surf. Coat. Technol.* **108-109**, 236 (1998).
- [13] M. Diserens, J. Patscheider, F. Lévy, *Surf. Coat. Technol.* **108-109**, 241 (1998).

- [14] S. Veprek, P. Nesládek, A. Niederhofer, F. Glatz, M. Jílek, M. Šíma, *Surf. Coat. Technol.* **108-109**, 138 (1998).
- [15] D. A. Glocker, S. I. Shah, *Handbook of Thin Film Process Technology*, IOP Publishing, Bristol and Philadelphia, Vol. 2, (1995).
- [16] H. Randhawa, *Surf. Coat. Technol.* **36** 829 (1988).
- [17] Y. Igasaki, H. Mitsuhashi, K. Azuma, T. Muto, *Jap. J. Appl. Phys.*, **17/1**, 85 (1978).
- [18] J.-E. Sundgren, B.-O. Johansson, S.-E. Karlsson, *Thin Sol. Films*, **105**, 353 (1983).
- [19] J.-E. Sundgren, B.-O. Johansson, S.-E. Karlsson, *Thin Sol. Films*, **105**, 367 (1983).
- [20] J. Stanislav, J. Sikac, M. Cermak, *Thin Solid Films*, **191**, 255 (1990).
- [21] F. Elstner, A. Ehrlich, H. Giegengack, H. Kupfer, F. Richter, *J. Vac. Sc. Techn.* **A 12**, 476 (1994).
- [22] G. Berg, C. Friedrich, E. Broszeit, K. H. Kloos, *Surf. Coat. Techn.*, **74-75**, 135 (1995).
- [23] M. Kawamura, Y. Abe, H. Yanagisawa, K. Sasaki, *Thin Sol. Films*, **287**, 115 (1996).
- [24] E. Ribeiro, A. Malczyk, S. Carvalho, L. Rebouta, J. V. Fernandes, E. Ailves, A. S. Miranda, *Surf. Coat. Technol* **151 – 152**, 515 (2002).
- [25] B. Window, N. Savides, *J. Vac. Sci. Technol.* **A 4**, 196 (1986).
- [26] G. G. Stoney, *Proc. Roy. Soc. (London)* **A 82**, 172 (1909).
- [27] F. Vaz, L. Rebouta, P. Goudeau, J. P. Rivière, M. Bodmann, G. Kleer, W. Döll, *Thin Solid Films* **402**, 195 (2002).
- [28] M. F. Doerner, W. D. Nix, *J. Mater. Res.* **1**, 397 (1992).
- [29] G. M. Pharr, W. C. Oliver, *MRS Bull.* **177**, 28 (1992).
- [30] I. N. Sneddon, *Int. J. Engng. Sci.* **3**, 47 (1965).
- [31] A. I. Gusev, *Physics-Uspokhi* **43**(1), 1 (2000).
- [32] Kohlscheen, H. -R. Stock, P. Mayr, *Surf. Coat. Technol* **120 – 121**, 740 (1999).
- [33] H. A. Wriedt, J. L. Murray, *Bull. Alloy Phase Diagrams*, **8/4**, 378 (1987).
- [34] K. Lu, M. L. Sui, R. Lück, *Nanostruct. Mat.* **4/4**, 465 (1994).
- [35] J. A. Thornton, *American Revue Materials Science* **7**, 239 (1977).
- [36] J. A. Sue, *Surf. Coat. Techn.*, **61**, 115 (1993).
- [37] H. Yoshihara, H. Mori, *J. Vac. Sci. Technol.* **16**, 1007 (1979).
- [38] A. Matthews, D. G. Teer, *Thin Solid Films* **73**, 367 (1980).
- [39] A. K. Suri, R. Nimmagadda, J. Amiguet, *Thin Solid Films* **72**, 529 (1980).
- [40] V. Poulek, J. Musil, V. Valvoda, R. Cerny, *J. Phys. D: Appl. Phys.* **21**, 1657 (1988).

*Corresponding author: muntean.d@unitbv.ro